Applied Physics Letters ARTICLE pubs.aip.org/aip/apl

Manipulation of the excitonic emission in few-layer CrSBr by magnetic order, strain, and electrostatic doping

Cite as: Appl. Phys. Lett. **128**, 212401 (2026); doi: 10.1063/5.0315822
Submitted: 9 December 2025 · Accepted: 4 May 2026 ·
Published Online: 26 May 2026

View Online Export Citation CrossMark

Junyang Chen,[1] Xiaohua Wu,[1,a)] Mingqiang Gu,[1] Shoujing Chen,[1] Yujun Zhang,[2] Yanan Dai,[1,3,4] Qihang Liu,[1,3,4] Yue Zhao,[1,3] and Mingyuan Huang[1,3,a)]

AFFILIATIONS

[1]Department of Physics, State Key Laboratory of Quantum Functional Materials, and Guangdong Basic Research Center of Excellence for Quantum Science, Southern University of Science and Technology, Shenzhen 518055, China
[2]School of Physics and Astronomy and Key Lab of Quantum Information of Yunnan Province, Yunnan University, Kunming 650091, China
[3]Guangdong Provincial Key Laboratory of Advanced Thermoelectric Materials and Device Physics, Southern University of Science and Technology, Shenzhen 518055, China
[4]Quantum Science Center of Guangdong–Hong Kong–Macao Greater Bay Area (Guangdong), Shenzhen 518045, China

[a)]**Authors to whom correspondence should be addressed:** wuxh3@sustech.edu.cn and huangmy@sustech.edu.cn

ABSTRACT

The two-dimensional (2D) magnetic material CrSBr has attracted significant interest for developing spin-based optoelectronic devices due to its unique magneto-optical properties. In this Letter, we report a systematic study on the photoluminescence (PL) of the high-energy excitons in few-layer CrSBr and the associated trions. Besides the broad excitonic emission peak (X_l) at around 1.34 eV, we also observed another strong excitonic emission peak (X_h) at around 1.37 eV in a hBN-encapsulated 2L sample, which splits into two peaks in 3L and more layered samples. The X_h exciton is associated with the transition between the top valence band and the second lowest conduction band, which is forbidden by inversion symmetry in 1L CrSBr. By applying inhomogeneous strain or constructing heterojunction, the X_h exciton can be brightened in 1L samples. In addition, we observed two trions associated with the split X_h excitons in electrostatically doped 3L CrSBr samples. By tuning the CrSBr sample into a ferromagnetic (FM) state, one of the trions shows enhanced intensity, which is more than 40 times that of the original exciton. Our results demonstrate that the excitonic emission in few-layer CrSBr can be effectively manipulated by magnetic order, strain, and electrostatic doping.

The discovery of intrinsic FM order down to the monolayer limit has stimulated intensive research interest in both fundamental physics and potential spintronics applications in the 2D limit.[1–9] The magneto-optical properties, magnetic excitations, and manipulation of magnetic order by pressure and electrostatic doping in van der Waals magnetic materials have been extensively investigated.[10–14] Recently, antiferromagnetic (AFM) semiconductor CrSBr has attracted a lot of attention due to many novel magneto-optical phenomena,[15–20] including anisotropic exciton emission coupled with magnetic order,[21–24] magnon–exciton coupling,[23,25,26] and exciton-polaritons.[27–29] Previous studies have demonstrated that both the energy and emission intensity of excitons can be modulated by the interlayer spin configuration.[22,30] However, existing literature presents conflicting results regarding the layer-dependent spectral features of the high-energy exciton (X_h) at 1.37 eV. Farsane *et al.* reported that the exciton X_h exists in 2L CrSBr and splits in samples with three or more layers. In contrast, Shao *et al.* reported that X_h appears only in three- or more-layer CrSBr and assigned it as a surface exciton.[30–32] Moreover, the intensity of the excitonic emission is relatively low, which limits the application of CrSBr in opto-spintronics.[33–36] Therefore, developing efficient methods to manipulate the optical activity of these excitons and improve their emission intensity in CrSBr is crucial for its future applications in spin-based optoelectronic devices.

In this Letter, we present a systematic study on the excitonic emission of hBN-protected few-layer CrSBr. By employing cryogenic

PL and differential reflectance spectroscopy, a bright high-energy exciton peak (X_h) at around 1.37 eV can be observed in hBN-encapsulated 2L CrSBr samples. This peak splits into two peaks in 3L and 4L samples, which are associated with excitons from surface and interior layers.[30] According to first-principles calculations, the high-energy exciton peak (X_h) is related to the transition between the second lowest conduction band and the top valence band, and this transition is forbidden by inversion symmetry in 1L CrSBr. By applying inhomogeneous strain or constructing a heterojunction to break the inversion symmetry, the dark exciton X_h in 1L CrSBr can be brightened. In addition, by using electrostatic doping, the trions associated with the high-energy exciton X_h are observed, and the intensity of the trion in 3L CrSBr can be enhanced by more than 40 times compared to the original exciton through magnetic order.

Figure 1(a) displays the PL spectra of 1–4L CrSBr samples are protected by hBN encapsulation at 1.7 K. The PL spectrum of the 1L sample only shows one asymmetric, broad peak at around 1.34 eV labeled as X_l, which evolved into a more complex feature in 2–4L samples; this low-energy excitonic transition originates from the topmost valence band (v) and the lowest conduction band (c_1) and has been demonstrated through a variety of experimental measurements.[22,30,31] In sharp contrast, a narrow and strong excitonic emission peak with a width of ~3 meV at about 1.37 (eV labeled as X_h) can be resolved in the 2L sample, and it splits into two peaks with a separation of ~5 meV (labeled as X_h') and X_h in the 3L and 4L samples. To confirm our observations, reflectance measurements are performed and the results are presented in Fig. 1(b). The high-energy excitonic transitions can be well resolved in differential reflectance spectra, which show excellent agreement with the PL spectra. In addition, the high-energy excitonic transitions become the dominant features in the reflectance spectra for 3L and 4L samples.

In previous studies, the appearance and origin of the X_h exciton peak remained controversial.[22,30–32] Farsane *et al.* reported that the X_h exciton appears in the PL spectrum of 2L samples and splits into two peaks in 3L samples,[30] while other groups have reported that the X_h exciton only exists in 3L or more-layer samples.[22,31,32] To investigate this issue, we prepared 2L and 3L CrSBr samples partially protected by hBN and partially exposed to air. Figures 1(d) and 1(e) show the PL spectra of the 2L and 3L samples from the hBN-protected (violet) area and exposed (green) area, respectively. Obviously, air exposure strongly suppresses the emission of the X_h exciton: the X_h exciton peak completely vanishes in the 2L sample, and only a single, low-intensity peak remains in the 3L sample. Our results demonstrate that hBN protection is essential for obtaining intrinsic PL spectra of few-layer CrSBr.

We next investigated the temperature dependence of the PL spectra of few-layer CrSBr samples. A representative result of 2L CrSBr sample is shown in Fig. 1(c) (the rest results are provided in supplementary material Fig. S1). As the temperature increases, the X_l peak shows a slight blueshift and loses its intensity at around 80 K; the

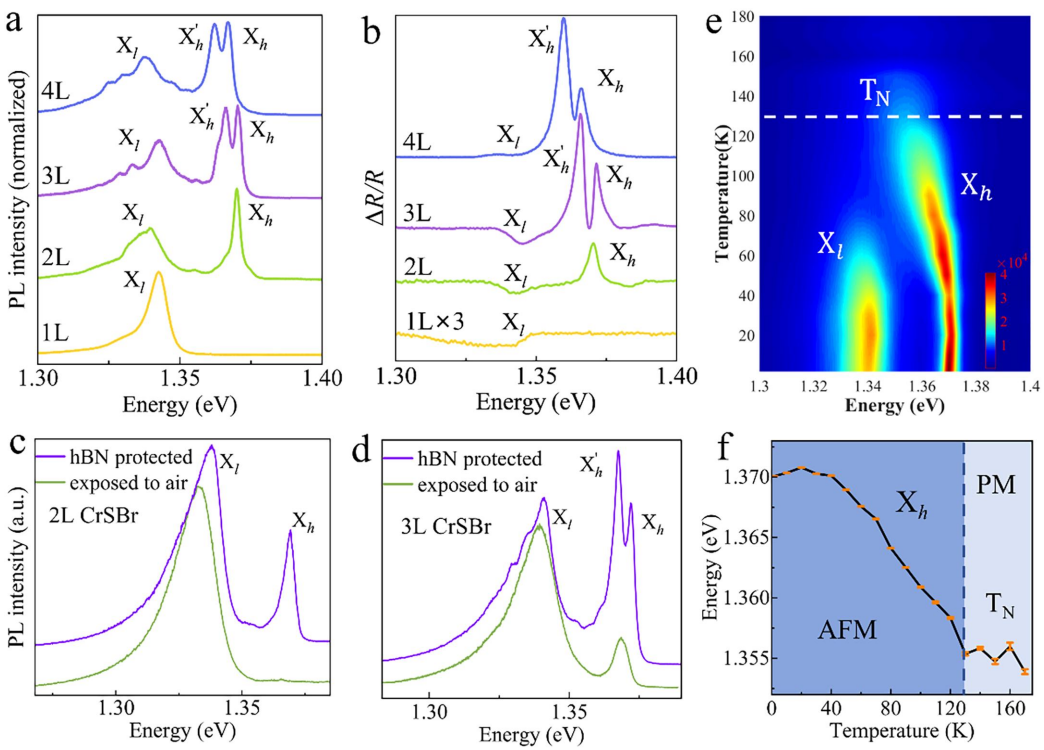

FIG. 1. Optical properties of hBN-protected few-layer CrSBr. (a) PL spectra of 1–4L CrSBr. For better illustration, the spectra are normalized with the maximum intensity. (b) Differential reflectance spectra of 1–4L CrSBr. 1L data are magnified threefold for clarity. PL spectra of 2L (c) and 3L (d) CrSBr with (violet) and without (green) hBN protection. (e) PL spectra of 2L CrSBr as a function of temperature. The white dashed line represents T_N (Néel temperature) for 2L CrSBr. (f) Temperature dependence of the X_h peak position. Dark blue highlights the AFM regions ($T < T_N$), while light blue indicates the paramagnetic regions.

X_h peak displays a minor blueshift below 40 K and then a clear redshift until the temperature approaches the Néel temperature (T_N) of 140 K. The peak positions of X_h are extracted by Lorentzian fitting and plotted in Fig. 1(f). In addition, the X_h peak shows clear broadening and a decrease in intensity above 40 K, and becomes broader and weaker above T_N.

To reveal the origin of the high-energy excitons in few-layer CrSBr samples, we performed first-principles GW calculations (details in Methods) to obtain the electronic band structure of 2L CrSBr in the AFM state, as shown in Fig. 2(a). Due to the combined symmetry of time reversal and spatial inversion, the band structure is degenerate in spins, which is almost the same as that of 1L CrSBr except for spin degeneracy. According to our calculations, the X_l exciton is assigned to the transition between the top valence band (v) and the lowest conduction band (c_1) around the Γ point, which is a dipole-allowed transition; the X_h exciton is assigned as the transition between the top valence band and the second lowest conduction band (c_2). From our analysis, the transition $v \rightarrow c_2$ is dipole-forbidden in 1L CrSBr due to spatial inversion symmetry, while this transition becomes dipole-allowed in 2L CrSBr because the AFM order breaks the inversion symmetry, as shown in Figs. 1(a) and 1(b).

For few-layer CrSBr, the intensity of the X_h exciton in the PL spectrum is similar to that of the X_l exciton, which is unusual because the c_1 band is much more populated than the c_2 band at low temperatures after excitation. To understand this phenomenon, the details of the c_1 and c_2 bands near the Γ point are magnified and plotted in Fig. 2(b), which shows that the minimum of the c_2 band is right at the Γ point and a direct optical transition can occur between the c_2 band and the v band, while the minimum of the c_1 band is slightly away from the Γ point, and the transition between the c_1 and v band is mostly indirect. Given the broadness of the X_l peak in the PL spectrum, it likely originates partially from indirect transitions and partially from direct transitions. In addition, the strong PL intensity of the X_h exciton in our protected CrSBr samples also requires a relatively slow relaxation rate from the c_2 band to the c_1 band, while the X_h exciton is undetectable in the unprotected 2L CrSBr sample, which may result from the increased relaxation rate after air exposure [see Figs. 1(c) and 1(d)].

Now, we turn to understand the PL spectrum in few-layer CrSBr under a magnetic field. The relevant energy bands and corresponding transitions for 1L and 2L CrSBr are simplified and summarized in Fig. 2(d). For 2L CrSBr, the c_1 and c_2 bands split into two sub-bands after changing from the AFM to FM state under the applied magnetic field, and this band splitting reduces the bandgaps for $v \rightarrow c_1$ and $v \rightarrow c_2$. Consequently, both X_l and X_h excitons display redshifts during the transition. Moreover, the FM order does not break inversion symmetry and the transition $v \rightarrow c_2$ becomes dipole-forbidden in the FM state, which is consistent with the observed significant decrease in intensity of the X_h exciton. Furthermore, the band splitting decreases the separation between the c_2 and c_1 sub-bands and hence increases the relaxation rate of $c_2 \rightarrow c_1$, which might be another important reason for the intensity decrease of the X_h' and X_h. In addition, the X_h exciton is still observable in the FM state as shown in Fig. 2(e), which means that the inversion symmetry breaking might not originate solely from the AFM magnetic order in 2L CrSBr and that interlayer mechanical coupling could be another possible reason.

Based on our analysis, the X_h exciton should also exist in 1L CrSBr as dark excitons due to inversion symmetry. To confirm our theory, we fabricated a 1L CrSBr sample on a SiO_2/Si substrate with a SiO_2 nanoparticle (diameter is about 1 μm) underneath the sample, as shown in Fig. 3(a). The adhesion between the sample and substrate produces inhomogeneous strain in CrSBr around the nanoparticle, which breaks its spatial inversion symmetry. The PL spectra of the 1L CrSBr sample were measured near (point B) and away from (point A) the nanoparticle and plotted in Fig. 3(b). The X_h exciton becomes a bright after inversion symmetry breaking. This result clarifies the

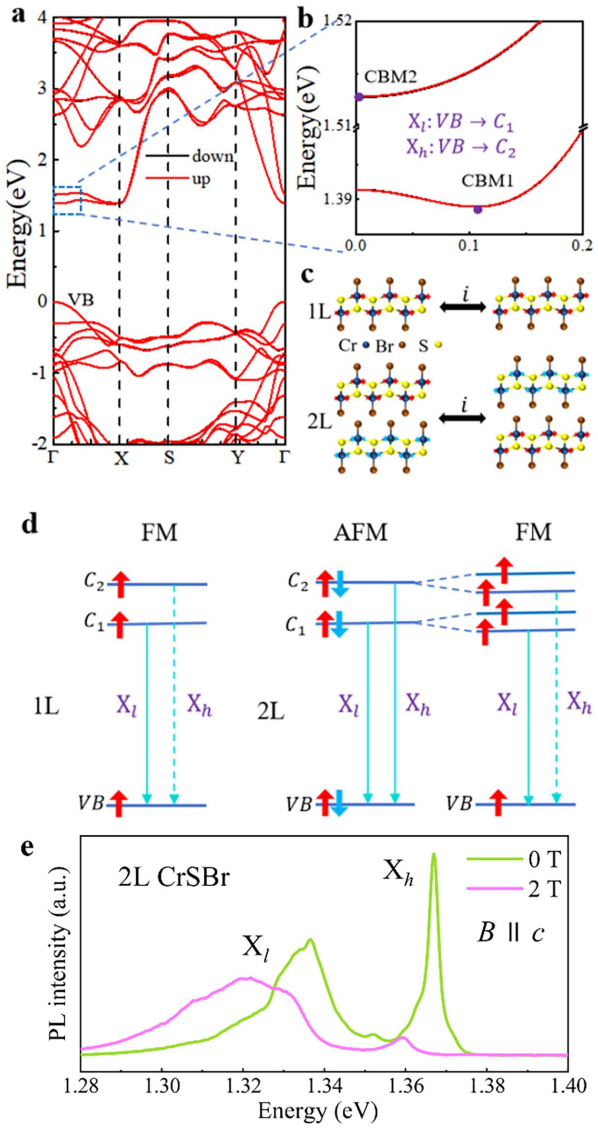

FIG. 2. (a) The electronic band structure of 2L CrSBr calculated using the GW method. (b) Enlarged band structure of two conduction bands near the Γ point, highlighting the conduction band minima of the first (CBM1) and second (CBM2) lowest conduction bands. (c) The spatial inversion symmetry in 1L and 2L CrSBr. (d) Optical transitions of 1L and 2L CrSBr in AFM and FM states. The solid lines with arrows denote dipole-allowed transitions, while the dashed lines with arrows indicate the dipole-forbidden transitions. (e) PL spectra of 2L CrSBr in the AFM and FM states.

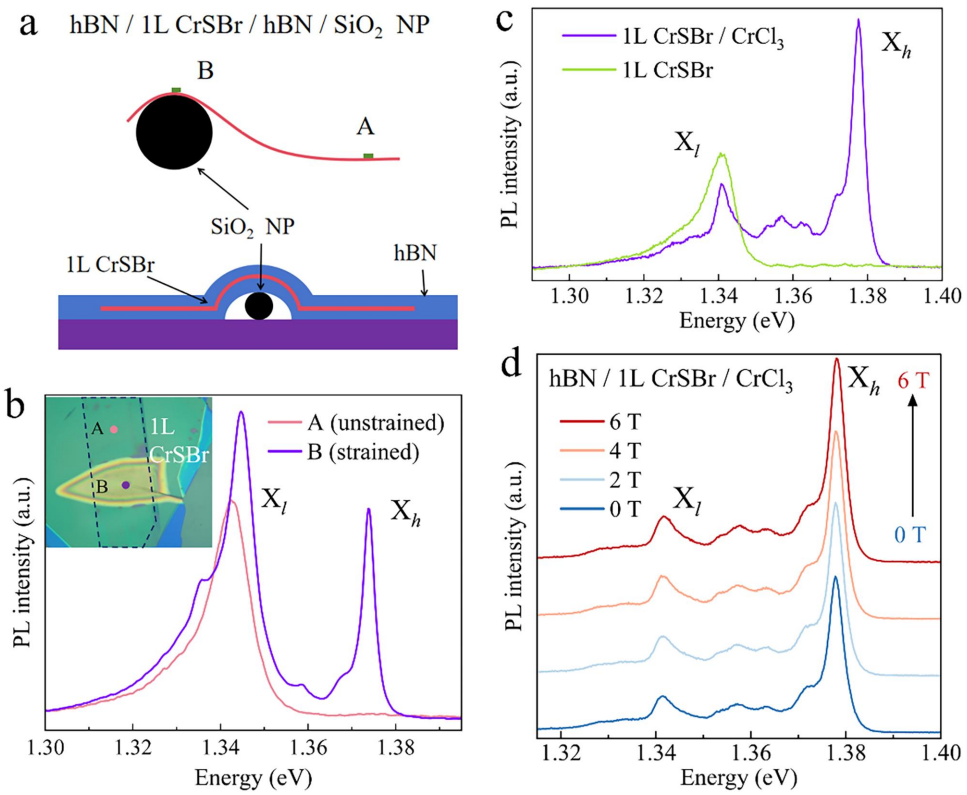

FIG. 3. Brightening of the dark exciton in 1L CrSBr. (a) Schematic illustration of strained 1L CrSBr device. NP denotes the nanoparticle. (b) The PL spectra of the intrinsic and inhomogeneously strained 1L CrSBr sample. The inset displays the optical image of the strained 1L CrSBr sample with marked measurement positions. (c) The PL spectra of the isolated 1L CrSBr (green) and 1L CrSBr/$CrCl_3$ heterojunction (violet). The thickness of $CrCl_3$ is around 3–5 nm. (d) Magnetic field dependence of the PL intensity of the 1L CrSBr/$CrCl_3$ heterojunction.

conflicting symmetry assignment of the c_1 and c_2 bands and demonstrates that the X_h exciton emission of 1L CrSBr can be modulated by controlling its symmetry.

Furthermore, by an fabricating hBN-protected 1L CrSBr/$CrCl_3$ heterojunction, the X_h exciton emission from 1L CrSBr can also be observed, as shown in Fig. 3(c). This observation can be understood by inversion symmetry breaking due to different interface interactions. To exclude alternative origins of the X_h exciton peak (e.g., from the 2L CrSBr), we measured the PL spectrum of the heterojunction under an external magnetic field up to 6T [Fig. 3(d)]. In contrast to the distinct peak redshifts and intensity decreases in the 2L sample [Fig. 2(e)], the PL spectra show no marked change in the 1L CrSBr/$CrCl_3$ heterojunction. Our results unambiguously demonstrate that the high-energy exciton X_h exists in 1L CrSBr as a dark exciton, which can be turned into a bright exciton by breaking inversion symmetry.

In addition to the brightening of the dark exciton in 1L CrSBr via strain and heterojunctions, modulation of the excitonic emission efficiency is also of great significance for advancing opto-spintronics.[35,36] In the following, we demonstrate the significant enhancement of the PL intensity by electrostatic gating in 3L CrSBr. We first fabricated a single-gated CrSBr device with its schematic side view shown in Fig. 4(a). The heterostructure is composed of a 3L CrSBr flake with a graphite contact, two hBN flakes as the protection layers, and a graphite top gate (see Methods). Figure 4(b) shows the evolution of the PL spectrum with the applied gate voltage (V_G) measured at 0 T. As V_G is continuously swept from −3 to +18 V, the emissions of the X_h and X_h' excitons are gradually suppressed and two new excitonic peaks gradually emerge about 20 meV below the X_h and X_h' excitons. These peaks display a slight redshift with increasing V_G and are assigned as the negatively charged X_h and X_h' excitons (trions), labeled as X_T and X_T', which is different from the previously reported single trion observed in 3L CrSBr.[30] To further confirm our assignment of the trions, we performed magneto-PL experiments with the gate voltage kept at 0 and +13 V and the results are shown in Figs. 4(c) and 4(d) and the supplementary material S4. The trion X_T (X_T') displays the same dispersive behavior as the exciton X_h (X_h'), while the trion X_T' (the exciton X_h') is more dispersive than the trion X_T (the exciton X_h). These results unambiguously demonstrate the origin of the trions.

As shown in Fig. 4(b), the trion X_T displays increasing intensity with increasing gate voltage V_G and similar maximal intensity to the exciton X_h, while the intensity of the trion X_T' is much higher than that of the exciton X_h' and is maximized at around 13 V. Furthermore, by tuning the AFM order into the fully polarized FM order through the magnetic field along the *c*-axis, the trion X_T'

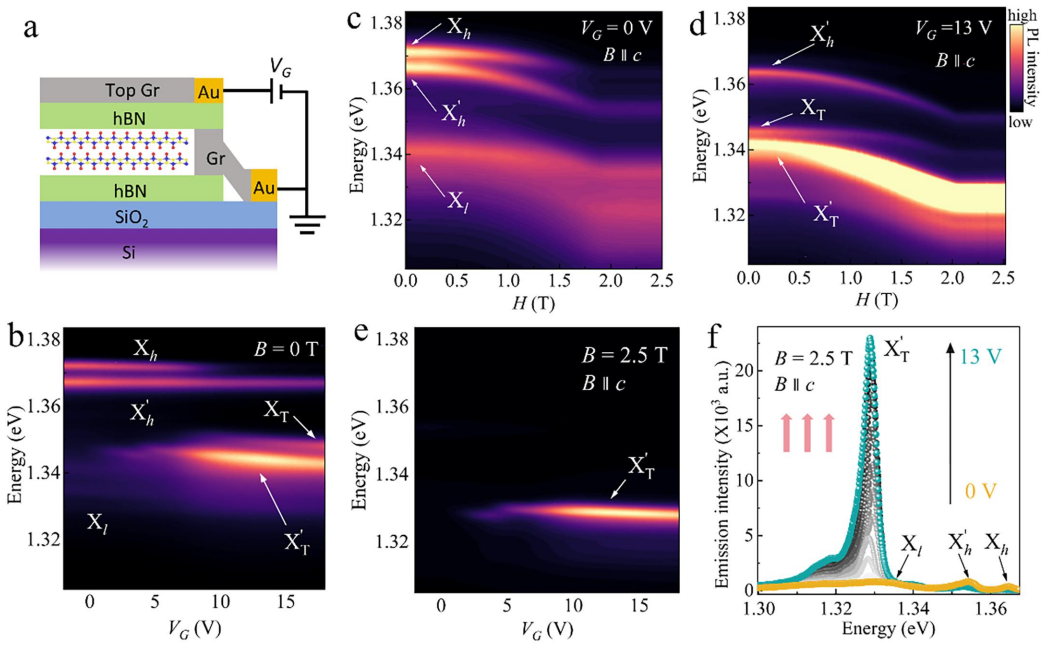

FIG. 4. (a) Schematic of the gated 3L CrSBr device. (b) PL spectra of 3L CrSBr as a function of the gate voltage V_G. PL spectra as a function of the magnetic field with a gate voltage V_G of 0 V (c) and 13 V (d), respectively. (e) and (f) PL spectra of 3L CrSBr under a magnetic field of 2.5 T as a function of the gate voltage V_G. The intensity of the trion X_T' can reach more than a 40-fold enhancement.

displays a substantial intensity enhancement and the intensity saturates at the FM state as shown in Fig. 4(d), while the intensity of the trion X_T is suppressed by the applied magnetic field. To further explore the intensity enhancement effect, we performed the electrostatic gating experiment in the FM 3L CrSBr sample and the results are plotted in Fig. 4(e). The trion X_T' arises and intensifies sharply as V_G increases until it approaches its maximum at around 13 V. However, its intensity is suppressed with further increase in the gate voltage V_G, which may be due to the high electric field-induced trion dissociation. The original excitons and the trion X_T merge into the background due to the high intensity of the trion X_T'. For a better illustration, Fig. 4(f) shows the PL spectra with increasing voltage, and the intensity of the negatively charged trion X_T' can reach more than 40 times that of the original exciton X_h'. We attribute this extraordinary enhancement to an energy crossover between X_T' and the low-energy exciton X_l. Initially, X_T' lies slightly above X_l in energy [Fig. 4(b)]. With increasing V_G, X_T' redshifts and the energy difference between X_T' and X_l almost vanishes [Fig. 4(b)]. On applying the magnetic field, X_T' undergoes a larger redshift than X_l [Figs. 4(c) and 4(d)], ultimately dropping below it. This energy crossover facilitates efficient population transfer into X_T', thereby dramatically boosting its emission intensity. In addition, our electrostatic gating measurements on 2L and 4L devices further support our explanation (see Fig. S5 in the supplementary material). The PL intensity increases by eight times for the 2L device and by 40 times for the 4L device. In 2L CrSBr, only the trion X_T (the charged X_h exciton) is present; while in 4L CrSBr, both trions X_T and X_T' exist. The energy of trion X_T' exhibits a larger redshift with magnetic field than that of the trion X_T, which leads to the 3L and 4L samples showing greater PL intensity enhancement than the 2L sample.

In summary, we have systematically studied the high-energy exciton X_h emission in hBN-protected few-layer CrSBr, which originates from the transition between the second lowest conduction band and the top valence band. This X_h exciton emission is optically forbidden by inversion symmetry in 1L CrSBr but can be brightened in unevenly strained samples. The high-energy exciton X_h splits into two excitons X_h and X_h' in 3L and more-layered samples. By using electrostatic doping, we observed two trions X_T and X_T' associated with the excitons X_h and X_h' in the 3L CrSBr sample. By tuning the CrSBr sample into FM state, the trion X_T' shows an enhanced intensity more than 40 times that of the original exciton, which could be explained by the energy crossover between the trion X_T' and the exciton X_l. Our results highlight the manipulation of excitonic emission in few-layer CrSBr by magnetic order, strain, and electrostatic doping, which may be useful in future opto-spintronic devices.

See the supplementary material for more details on experiments and computations, temperature-dependent PL, magneto-PL of few-layer CrSBr samples, magnetic field-dependent PL energies of excitons and trions, and electrostatic doping-induced enhancement of PL intensity in 2L and 4L CrSBr.

This work was supported by the National Natural Science Foundation of China (Grant Nos. 12074165, 12104204, 12374223, 92477108, and 11674150), the Guangdong Provincial Key Laboratory of Advanced Thermoelectric Materials and Device Physics (Grant No. 2024B1212010001), and the Shenzhen Science

and Technology Program (Grant Nos. 20231117151322001 and KQTD20240729102026004).

AUTHOR DECLARATIONS

Conflict of Interest

The authors have no conflicts to disclose.

Author Contributions

Junyang Chen: Conceptualization (equal); Data curation (equal); Formal analysis (equal); Investigation (equal); Methodology (equal); Project administration (equal); Software (equal); Validation (equal); Visualization (equal); Writing – original draft (equal); Writing – review & editing (equal). **Xiaohua Wu:** Conceptualization (equal); Data curation (equal); Formal analysis (equal); Investigation (equal); Methodology (equal); Project administration (equal); Software (equal); Supervision (equal); Validation (equal); Visualization (equal); Writing – original draft (equal); Writing – review & editing (equal). **Mingqiang Gu:** Conceptualization (equal); Data curation (equal); Funding acquisition (equal); Investigation (equal); Methodology (equal); Resources (equal); Software (equal). **Shoujing Chen:** Investigation (equal); Methodology (equal); Writing – review & editing (equal). **Yujun Zhang:** Investigation (equal); Methodology (equal). **Yanan Dai:** Funding acquisition (equal); Investigation (equal); Validation (equal); Writing – review & editing (equal). **Qihang Liu:** Data curation (equal); Funding acquisition (equal); Investigation (equal); Supervision (equal); Validation (equal). **Yue Zhao:** Data curation (equal); Funding acquisition (equal); Investigation (equal); Supervision (equal); Validation (equal). **Mingyuan Huang:** Conceptualization (equal); Formal analysis (equal); Funding acquisition (equal); Project administration (equal); Resources (equal); Supervision (equal); Writing – original draft (equal); Writing – review & editing (equal).

DATA AVAILABILITY

The data that support the findings of this study are available from the corresponding authors upon reasonable request.

REFERENCES

[1]C. Gong, L. Li, Z. Li, H. Ji, A. Stern, Y. Xia, T. Cao, W. Bao, C. Wang, and Y. Wang, Nature **546**(7657), 265–269 (2017).
[2]B. Huang, G. Clark, E. Navarro-Moratalla, D. R. Klein, R. Cheng, K. L. Seyler, D. Zhong, E. Schmidgall, M. A. McGuire, and D. H. Cobden, Nature **546**-(7657), 270–273 (2017).
[3]Y. Deng, Y. Yu, Y. Song, J. Zhang, N. Z. Wang, Z. Sun, Y. Yi, Y. Z. Wu, S. Wu, and J. Zhu, Nature **563**(7729), 94–99 (2018).
[4]Z. Fei, B. Huang, P. Malinowski, W. Wang, T. Song, J. Sanchez, W. Yao, D. Xiao, X. Zhu, and A. F. May, Nat. Mater. **17**(9), 778–782 (2018).
[5]K. S. Burch, D. Mandrus, and J.-G. Park, Nature **563**(7729), 47–52 (2018).
[6]T. Song, X. Cai, M. W.-Y. Tu, X. Zhang, B. Huang, N. P. Wilson, K. L. Seyler, L. Zhu, T. Taniguchi, and K. Watanabe, Science **360**(6394), 1214–1218 (2018).
[7]D. R. Klein, D. MacNeill, J. L. Lado, D. Soriano, E. Navarro-Moratalla, K. Watanabe, T. Taniguchi, S. Manni, P. Canfield, and J. Fernández-Rossier, Science **360**(6394), 1218–1222 (2018).
[8]C. Gong and X. Zhang, Science **363**(6428), eaav4450 (2019).
[9]W. Chen, Z. Sun, Z. Wang, L. Gu, X. Xu, S. Wu, and C. Gao, Science **366**-(6468), 983–987 (2019).
[10]S. Jiang, J. Shan, and K. F. Mak, Nat. Mater. **17**(5), 406–410 (2018).
[11]T. Li, S. Jiang, N. Sivadas, Z. Wang, Y. Xu, D. Weber, J. E. Goldberger, K. Watanabe, T. Taniguchi, and C. J. Fennie, Nat. Mater. **18**(12), 1303–1308 (2019).
[12]T. Song, Z. Fei, M. Yankowitz, Z. Lin, Q. Jiang, K. Hwangbo, Q. Zhang, B. Sun, T. Taniguchi, and K. Watanabe, Nat. Mater. **18**(12), 1298–1302 (2019).
[13]B. Huang, G. Clark, D. R. Klein, D. MacNeill, E. Navarro-Moratalla, K. L. Seyler, N. Wilson, M. A. McGuire, D. H. Cobden, and D. Xiao, Nat. Nanotechnol. **13**(7), 544–548 (2018).
[14]S. Jiang, L. Li, Z. Wang, K. F. Mak, and J. Shan, Nat. Nanotechnol. **13**(7), 549–553 (2018).
[15]K. Lee, A. H. Dismukes, E. J. Telford, R. A. Wiscons, J. Wang, X. Xu, C. Nuckolls, C. R. Dean, X. Roy, and X. Zhu, Nano Lett. **21**(8), 3511–3517 (2021).
[16]Z. Sun, C. Hong, Y. Chen, Z. Sheng, S. Wu, Z. Wang, B. Liang, W.-T. Liu, Z. Yuan, and Y. Wu, Nat. Mater. **24**, 226–233 (2025).
[17]D. Wu, Y. Xu, M. Ye, and W. Duan, Sci. Adv. **11**(14), eadu6562 (2025).
[18]C. Wang, X. Guo, Z. Zhai, M. Cheng, S.-W. Cheong, A. W. Tsen, B. Lv, and L. Zhao, arXiv:2509.13542 (2025).
[19]Y. Zhai, Y. Tang, T. Zhou, H. Li, T. Qin, Z. Sofer, L. Hu, and Q. Xiong, Nano Lett. **25**(33), 12570–12577 (2025).
[20]K. Torres, A. Kuc, L. Maschio, T. Pham, K. Reidy, L. Dekanovsky, Z. Sofer, F. M. Ross, and J. Klein, Adv. Funct. Mater. **33**(12), 2211366 (2023).
[21]J. Klein, B. Pingault, M. Florian, M.-C. Heißenbüttel, A. Steinhoff, Z. Song, K. Torres, F. Dirnberger, J. B. Curtis, and M. Weile, ACS Nano **17**(6), 5316–5328 (2023).
[22]N. P. Wilson, K. Lee, J. Cenker, K. Xie, A. H. Dismukes, E. J. Telford, J. Fonseca, S. Sivakumar, C. Dean, and T. Cao, Nat. Mater. **20**(12), 1657–1662 (2021).
[23]G. M. Diederich, J. Cenker, Y. Ren, J. Fonseca, D. G. Chica, Y. J. Bae, X. Zhu, X. Roy, T. Cao, and D. Xiao, Nat. Nanotechnol. **18**(1), 23–28 (2023).
[24]J. Cenker, S. Sivakumar, K. Xie, A. Miller, P. Thijssen, Z. Liu, A. Dismukes, J. Fonseca, E. Anderson, and X. Zhu, Nat. Nanotechnol. **17**(3), 256–261 (2022).
[25]Y. J. Bae, J. Wang, A. Scheie, J. Xu, D. G. Chica, G. M. Diederich, J. Cenker, M. E. Ziebel, Y. Bai, and H. Ren, Nature **609**(7926), 282–286 (2022).
[26]Q. Li, X. Xie, A. Alfrey, C. W. Beach, N. McLellan, Y. Lu, J. Hu, W. Liu, N. Dhale, and B. Lv, Phys. Rev. Lett. **133**(26), 266901 (2024).
[27]F. Dirnberger, J. Quan, R. Bushati, G. M. Diederich, M. Florian, J. Klein, K. Mosina, Z. Sofer, X. Xu, and A. Kamra, Nature **620**(7974), 533–537 (2023).
[28]T. Wang, D. Zhang, S. Yang, Z. Lin, Q. Chen, J. Yang, Q. Gong, Z. Chen, Y. Ye, and W. Liu, Nat. Commun. **14**(1), 5966 (2023).
[29]L. Nessi, C. A. Occhialini, A. K. Demir, L. Powalla, and R. Comin, ACS Nano **18**(50), 34235–34243 (2024).
[30]F. Tabataba-Vakili, H. P. Nguyen, A. Rupp, K. Mosina, A. Papavasileiou, K. Watanabe, T. Taniguchi, P. Maletinsky, M. M. Glazov, and Z. Sofer, Nat. Commun. **15**(1), 4735 (2024).
[31]K. Lin, Y. Li, M. Ghorbani-Asl, Z. Sofer, S. Winnerl, A. Erbe, A. V. Krasheninnikov, M. Helm, S. Zhou, and Y. Dan, J. Phys. Chem. Lett. **15**(23), 6010–6016 (2024).
[32]Y. Shao, F. Dirnberger, S. Qiu, S. Acharya, S. Terres, E. J. Telford, D. Pashov, B. S. Kim, F. L. Ruta, and D. G. Chica, Nat. Mater. **24**, 391–398 (2025).
[33]Y. Wang, S. Yang, L. Huang, Y. Ran, P. Gu, X. Huang, K. Watanabe, T. Taniguchi, Z. Chen, and Y. Ye, Adv. Funct. Mater. **36**, e16052 (2025).
[34]F. Qin, H. Liu, A. Yang, Y. Liu, X. Wang, Y. Sun, X. Zhou, Z. Sofer, J. Zhou, and X. Liu, arXiv:2508.00572 (2025).
[35]S. Mouri, Y. Miyauchi, and K. Matsuda, Nano Lett. **13**(12), 5944–5948 (2013).
[36]H. Nan, Z. Wang, W. Wang, Z. Liang, Y. Lu, Q. Chen, D. He, P. Tan, F. Miao, and X. Wang, ACS Nano **8**(6), 5738–5745 (2014).